

The Assessment of Relative Permittivity on Diesel Vapour in the Moisture Content of Terap Red Soil by Ground Penetrating Radar

Authors: Ghazali, Mimi Diana, Zainon, Othman, M.Idris, Khairulnizam, Zainon, Siti Nor Ain, A Karim, Mohd Nazri, et al.

Source: Air, Soil and Water Research, 13(1)

Published By: SAGE Publishing

URL: <https://doi.org/10.1177/1178622120930661>

BioOne Complete (complete.BioOne.org) is a full-text database of 200 subscribed and open-access titles in the biological, ecological, and environmental sciences published by nonprofit societies, associations, museums, institutions, and presses.

Your use of this PDF, the BioOne Complete website, and all posted and associated content indicates your acceptance of BioOne's Terms of Use, available at www.bioone.org/terms-of-use.


Usage of BioOne Complete content is strictly limited to personal, educational, and non - commercial use. Commercial inquiries or rights and permissions requests should be directed to the individual publisher as copyright holder.

BioOne sees sustainable scholarly publishing as an inherently collaborative enterprise connecting authors, nonprofit publishers, academic institutions, research libraries, and research funders in the common goal of maximizing access to critical research.

The Assessment of Relative Permittivity on Diesel Vapour in the Moisture Content of Terap Red Soil by Ground Penetrating Radar

Air, Soil and Water Research
Volume 13: 1–11
© The Author(s) 2020
Article reuse guidelines:
sagepub.com/journals-permissions
DOI: 10.1177/1178622120930661



Mimi Diana Ghazali^{1,2} , Othman Zainon², Khairulnizam M. Idris², Siti Nor Ain Zainon³, Mohd Nazri A Karim⁴, Siti Aminah Anshah¹ and NoorFatekah Abdul Talib¹

¹Centre of Studies for Surveying Sciences and Geomatics, Faculty of Architecture, Planning & Surveying, Universiti Teknologi MARA, Arau, Malaysia. ²Department of Geoinformation, Faculty of Built Environment and Surveying, Universiti Teknologi Malaysia, Skudai, Malaysia. ³Center of Foundation Studies, Universiti Islam Antarabangsa Sultan Abdul Halim Mu'adzam Shah, Kuala Ketil, Malaysia. ⁴Department of Electronic Engineering, Faculty of Engineering Technology, UNICITI ALAM, Universiti Malaysia Perlis, Padang Besar, Malaysia.

ABSTRACT: In a common agriculture resource, soil contamination monitoring is a prominent area of study. Nowadays, it is crucial to provide a database for the interpretation of ground penetrating radar (GPR) field data in monitoring soil contamination, such as diesel scatter migration. This study aims to assess the association between permittivity properties and soil water content (θ_w) for diesel contamination in Terap Red soil, which is classified as lateritic soil. Terap Red soil is an agro potential soil and available in more than 40% of distribution areas in Northern Malaysia (Agro-based State). In this research, 800 MHz shielded antenna GPR was applied for 24 hour measurement in a concrete simulation field tank, which was filled with Terap Red soil (1.5 m x 2.6 m x 1.5 m) located at Universiti Teknologi MARA (UiTM) Perlis, Malaysia. Embedded moisture content probe was simultaneously measured to monitor the response of volumetric water content in the contaminated soil. The GPR data were pre-processed and filtered by Reflexw 7.5. The calibrated Agilent Technologies Automated Vector Analyser (VNA) was used to verify the independent relative permittivity value from GPR. As a result, the evaluation of velocities and reflection of GPR data were influenced by the presence of diesel and contaminated vapour. A positive and significant correlation was obtained between relative permittivity and moisture content in the diesel-contaminated soil. In addition, a positive and strong linear regression analysis was also found between relative permittivity and moisture content. This analysis included an accurate total difference of root mean square error (RMSE) difference, which amounted to 0.04, with calibrated dielectric permittivity.

KEYWORDS: Soil pollution, GPR anomalies, degradation, permittivity calibration

RECEIVED: April 30, 2020. **ACCEPTED:** May 2, 2020.

TYPE: Original Research

FUNDING: The author(s) received no financial support for the research, authorship, and/or publication of this article.

DECLARATION OF CONFLICTING INTERESTS: The author(s) declared no potential conflicts of interest with respect to the research, authorship, and/or publication of this article.

CORRESPONDING AUTHOR: Mimi Diana Ghazali, Centre of Studies for Surveying Sciences and Geomatics, Faculty of Architecture, Planning & Surveying, Universiti Teknologi MARA, Arau Campus, 02600 Arau, Perlis, Malaysia. Email: mimidiana@uitm.edu.my

Introduction

Permittivity properties are the ratio of the electric-field storage capacity for a material.¹ Meanwhile, electrical conductivity refers to the potential of the soil conduct electric current.² Soil permittivity properties and soil electric conductivity are highly associated with soil moisture content. Many researchers, including Topp,³ Brevik et al⁴ and Karim et al⁵ observed a strong positive correlation between the permittivity constant and volumetric water content of soils with various textures. Sun et al⁶ presumed that the magnitude of electric conductivity increased with the increase in soil moisture. However, the presence of hydrocarbon in the soil will replace the water retained by the soil and be trapped in the soil particle, which indirectly affected the permittivity value.

Darayan et al⁷ assessed the transformations occurring in the electric properties of diesel-contaminated soil with a guarded-electrode and a parallel-plate sample holder. As a result, the replacement rates were influenced by the density, viscosity of hydrocarbon, and soil textures. A study by Ijimdiya⁸ showed

that increased oil content changed the aggregate size distribution curve from finer to coarser. Similarly, Naqvi et al⁹ and Bortoni et al¹⁰ found that the presence of hydrocarbons, such as methane, diesel fuel, and propane led to a negative influence in the soil moisture content. Overall, it could be said that several investigations have been done on the correlation between electric properties and soil contamination through a geophysical method, such as GPR.

Many researchers, including Glaser et al,¹¹ Mansi et al¹² and Shao et al,¹³ claimed that detecting soil contaminant through the GPR as a non-destructive measurement was an effective methodology to solve environmental issues. However, the penetration of the GPR into the soil contaminant depended on the change in the permittivity and permeability of soil moisture. While soil texture could affect the reflection of the electromagnetic waves (EM), these waves were reduced by conductivity.¹⁴ The wave propagation velocity might have been obtained from electrical conductivity and permittivity.^{12,15-17} Furthermore, Daniels et al¹⁸ stated that the wave propagation velocity is due



Creative Commons Non Commercial CC BY-NC: This article is distributed under the terms of the Creative Commons Attribution-NonCommercial 4.0 License (<https://creativecommons.org/licenses/by-nc/4.0/>) which permits non-commercial use, reproduction and distribution of the work without further permission provided the original work is attributed as specified on the SAGE and Open Access pages (<https://us.sagepub.com/en-us/nam/open-access-at-sage>).
Downloaded From: <https://bioone.org/journals/Air,-Soil-and-Water-Research> on 18 Apr 2024
Terms of Use: <https://bioone.org/terms-of-use>

to the vapour phase of the gasoline, leading to water displacement in the vadose zone, which is formed as a hydrocarbon float. As a result, the reflection from sedimentary features is diminished. Meanwhile, Alsharahi et al,¹⁴ highlighted that the notable reduction of GPR reflection effects is possibly due to higher electrical conductivity, such as clay soil.

However, more studies were conducted on the relationship between soil moisture and soil electrical properties without the presence of hydrocarbon contamination and light non-aqueous phase liquids (LNAPLs) for the clay and sand type of soil. Shao et al,¹³ performed a 24 hour GPR monitoring on the diesel fuel as a hydrocarbon in the category of liquid non-aqueous phase liquid (LNAPLs) in coarse quartz sands, and it was found that the diesel had an impact on the GPR reflected energy. Numerical modelling was used by Bano et al¹⁹ to generate GPR modelling with permittivity property mixing models so that the physical attributes and volume of the diesel-contaminated sand were evaluated.

By the literature, perceived that distribution of different non-aqueous phase liquids (NAPLs) in the different soil can be very complex and may change every time depending on soil type and contamination. Thus, the GPR approach from literature was limited to the specific soil texture, porosity conditions and chemical reaction of NAPLs. As the result, relative permittivity studies on diesel contaminated Terap Red soil in GPR reflection most crucial seeing that Terap Red soil has its own soil characteristic. To partially fill the gap, in this study we comply a series of VNA calibration experiments aiming to extend the reliability of GPR identification of contaminated soils.

This study aims to conduct a detailed investigation of the effectiveness of GPR ability to assess the migration of diesel scatter and evaluate the association between permittivity and soil water content (θ_w) for diesel-contaminated Terap Red soil. Then, through a series of fieldwork from contaminated soil tank, diesel fuel is believed to affect soil moisture content and while varying the reflectivity of the GPR and permittivity of contaminated soil. We hypothesised that the contamination of terap soil by diesel oil leads to increased soil water repellency, which result in increasing volumetric water content and will be contributed to changes of permittivity for diesel contamination in Terap Red soil.

Materials and Method

Material

Infiltration experiment was performed in a large-scale tank with a size of 1.5 m x 2.6 m x 1.5 m and 5 cm thickness. It was constructed from concrete block filled with soil. The use of the concrete block as a high conductivity material²⁰ is due to the consideration over the reduction of EM wave reflection effects and the controlled propagation of EM wave over the boundary of simulation site, which distinguishes the areas between simulation sites. This tank was located at UiTM Perlis (as shown in Figure 1) within an ambient temperature at a monthly average

of 30°C/24°C with un-controlled moisture. Furthermore, the polyvinyl chloride (PVC) pipe in the tank had a diameter was 4.5 cm. It was located 0.5 m below from the top and along the soil tank to simulate diesel leak in the centre of PVC pipeline with 3 cm diameter. The release volume of diesel leak in 30 litres. Kinematic viscosity @ 40°C of diesel was 4.0 cSt, while density @ 15°C: 0.8443 kg/L, carbon residue (10% residue): < 0.1 wt%, water by distillation: < 0.05 vol%, respectively.

To conduct precise monitoring of leak migration, the diesel was poured into Terap Red soil medium all at once. Terap Red soil is a part of the laterite soil family group, which is classified by USDA Soil Taxonomy as clayey-skeletal, kaolinitic, typic pelaudult, and isohyperthermic.²¹ The soil colour consists of a range from yellowish-brown to dark brown, including clayey gravel and medium-deep, with a depth ranging from 25 to 75 cm. In relation to the aforementioned characteristics, as a major group of soil from the coastal districts of Northern Malaysia, Terap Red soil is suitable for agricultural purposes, such as 'Harum Manis mango' (the second largest food crop production after paddy cultivation in Northern Malaysia). In this research, Terap Red soil filling was obtained from an area located in the Harum Manis cultivation of Agrotechnology Farm, UiTMPs (6.2659 N, 100.1648 E). Particle size range from 2 to 0.015 mm was obtained from the sieved analysis of grain size distribution, which was based on BS 1377-2:1990.²²

Data collection

The research was based on ground penetrating radar (GPR) measurement, which was conducted from a simulation testbed in order to measure the permittivity constant (ϵ_r) values and evaluate the changes related to the variation of moisture content. GPR measurement was collected using a high 800 MHz shielded antenna. The shielded antenna was operated in a common offset (CO) GPR survey method with a MALA GroundVision 2 acquisition software system and ProEx control unit. Notably, the acquisition software system was built by the Mala Geoscience AB of Guideline Geo. After the experiment with 50 cm space lines (as shown in Figure 2A and B), the measurement was carried out on 5 profile lines along a single transect at the site during 25 tests, which were conducted repeatably for every 1 hour within 24 hours with the same setting parameter for GPR measurement. For an optimum collection of GPR data, the 2.6 m trace, with each of the four rows being set apart by 0.5 m, was nominally traced. Moreover, the measurement was performed on a single-offset 2D section using the setting parameters suggested by the manufacturer, including the increase in antenna separation by 0.14 m, 512 samples, a time window of 52.4128 ns, the vertical stack at eightfold, a sampling frequency of 9600 MHz, and a trig interval of 0.01 m. Due to antenna separation, the zero value for the depth scale was calculated using the first arrival of 10 samples, including the adjusted first arrival within the travel time and the velocity of 100 m per microsecond (μ s).

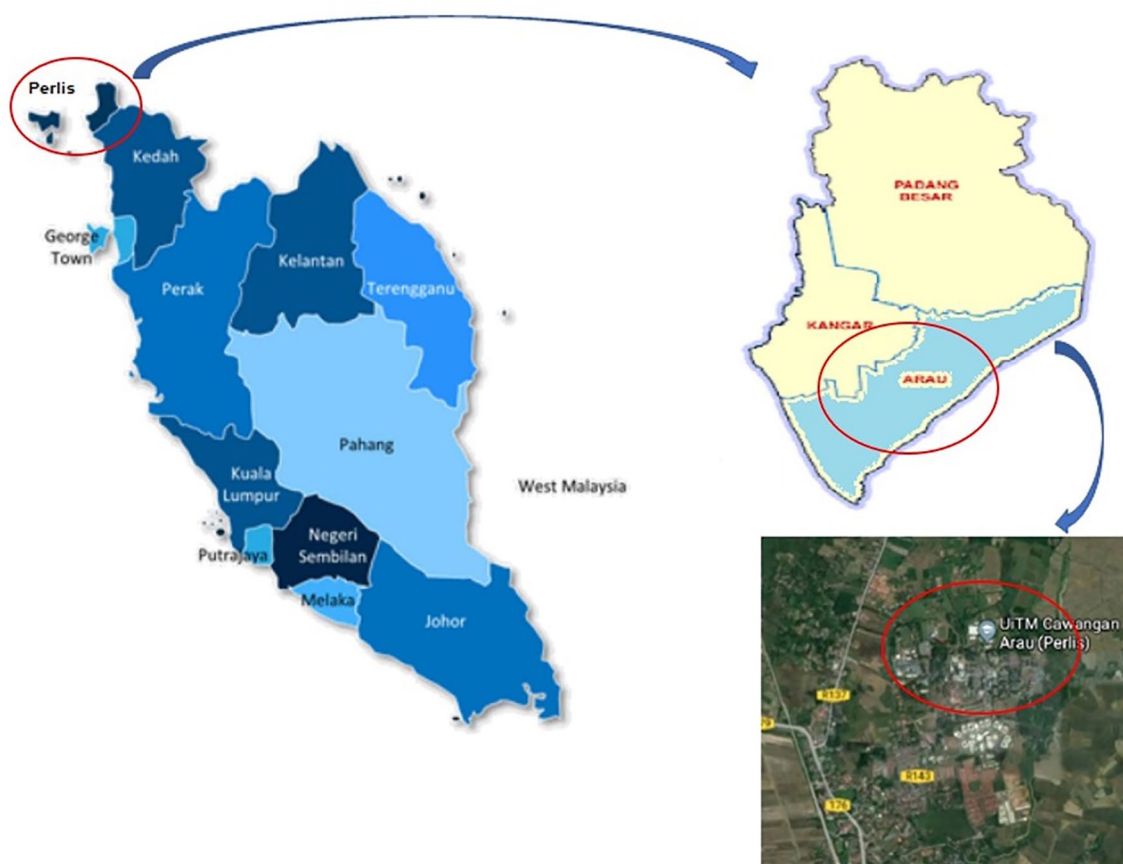


Figure 1. The location map of the concrete block tank filled with diesel contamination in Terap Red soil for infiltration experiment, located at Universiti Teknologi MARA, Perlis.

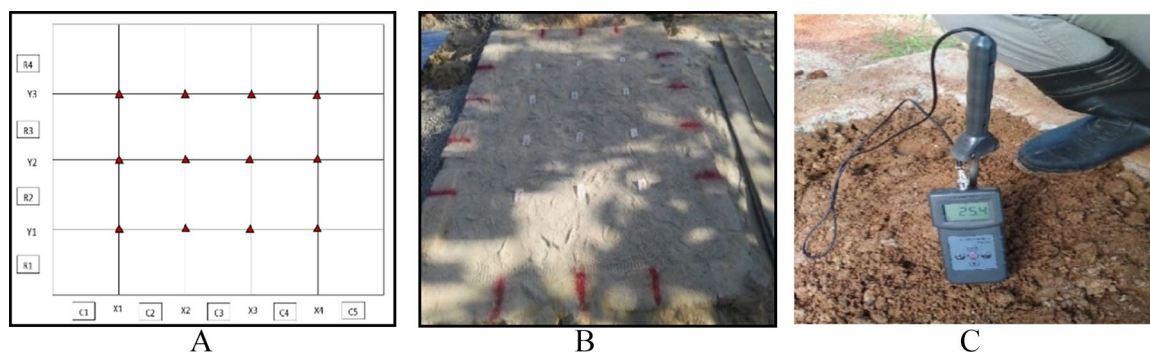


Figure 2. The GPR measurement (A) gridline with the interval of 0.5m for each grid and scanning direction, (B) the gridline marked on the concrete block which was filled with fine sand, and (C) the moisture content probe test. GPR indicates Ground Penetrating Radar.

Calibration of the distance measuring instrument, which was also known as a wheel calibration, was performed on a calibration line which was 10m long on the ground surface. This process aimed to increase the locational reliability and accuracy of GPR measurement. However, it should be noted that the percentage of the survey wheel distance error must not exceed $<2\%$. Besides, the depth calibration should also be done to maintain the precision of the depth. In a scale setting, the velocity parameter was set for each line on the equipment prior to the measurement. Radar velocities were calculated based on the speed of the electromagnetic wave, V_m (equation

2). Meanwhile, manual stake measurement was used to calibrate the radargrams in the REFLEXWTM.

Soil moisture content (θ_w) was measured simultaneously during GPR measurement on soil contamination with the metre of soil moisture probe amounted to PMS710 (refer to Figure 2 C). The probe was placed at the contaminated area to optimise the affected soil moisture to GPR reflection measurement. The calibrated θ_w from the probe was conducted in laboratory analysis using gravimetric water content (GWC) method based on the standard procedure of classification test in British Standard BS 1377-2:1990. The soil sample was dried

Table 1. GPR processing parameters used for Terap Red soil scanning with Reflexw Software.

PROCESS	PARAMETER
Time zero	−2.040 ns
S/R Distance	0.18 m
Dewow	52.4128 ns
Bandpass Butterworth Filter	600-1200
Gain function	7 db/m
Hyperbola fitting	0.0639 ns

Abbreviation: GPR, ground penetrating radar.

at 105°C for 24 hours. The θ_w calculation of the soil specimen, w , as a dry soil mass (m) percentage which was nearest to 0.1%, is presented in the following equation

$$w = \left(\frac{m_2 - m_3}{m_3 - m_1} \right) 100(\%) \quad (1)$$

where w is the moisture content expressed as a percentage, m_1 is the weight of the container, m_2 is the weight of the container + weight of moist soil, and m_3 is the weight of the container + weight of the dry soil.

GPR basic processing and interpretation

Prior to the production of time/depth section and data analysis, the data were filtered during data processing by REFLEXW™ software. This process was performed to enhance the features of the hyperbola and remove the background and ambient noise. The raw data, as recorded in *MALA GroundVision 2*, were imported into REFLEXW™ for GPR data processing and interpretation. A summary of the processing parameters applied for GPR data is presented in Table 1. Furthermore, the initial basic data processing to the GPR dataset started with editing the header file. Before any processing was conducted, it was preferable for the header files of each section to be viewed in sequence to verify the consistency of the survey parameters. Following are the flow of the next post-acquisition processing operation, which is (1) time zero correction, (2) dynamic correction, (3) background removal, (4) dewow filtering, (5) automatic gain function, (6) bandpass filtering, and (7) hyperbola fitting. The basic descriptions of the processing flow used for the analysis of GPR data using ReflexW are as follows:

- Time zero correction: To remove the time delay of the first waveform arrival from the transmitter to the receiver so that the vertical position is controlled.²³
- Dynamic correction: To rectify the effects of antenna offset by the variable time shift within a trace.

- Background removal: To eliminate the background noise occurring in a horizontal position during the phenomenon of antenna ringing in the GPR data.
- Dewow filter: To eliminate the elements of DC signal, also referred to as DC bias, and significantly low-frequency signal trend in the data, which was also known as a ‘wow’ effect.²⁴
- Automatic Gain Control: To emphasise low amplitudes opposite of high amplitudes which improve data display and interpretation.
- Bandpass Filter: To remove unwanted frequency based on technical specification parameter by cleaning up significantly low- and high-frequency noise using bandpass filtering.²⁵
- Hyperbola Fitting: To generate velocity model and accurate hyperbola gain which are essential for precise depth measurement and improved tomography.

Calculation of soil relative permittivity from GPR signal

The moisture measurement from GPR data was estimated based on the identification of the relative permittivity of diesel contamination in Terap Red soil. The determination of the relative permittivity was also identified as the association between the velocity of an EM wave in medium (v) and the velocity of an EM wave in a vacuum which was based on the speed of light in free space ($c=0.3$ m/ns). The relationship was described by the following equation

$$V_m = \frac{c}{\sqrt{(\epsilon_r \mu_r)}} \quad (2)$$

Based on the assumption of a low-loss material in Terap Red soil, the simplified version of equation 2 was obtained from the following equation

$$V_m = \frac{c}{\sqrt{(\epsilon_r \mu_r) + ((1 + P^2) + 1)}} \quad (3)$$

Based on the above equation, assuming that relative magnetic permeability ($\mu_r=1$ for non-magnetic materials) was near to unity²⁶ and loss factor, P was considered as 0 value ($P \approx 0$).

Statistical analysis

Relationship of the permittivity and moisture content was accessed by linear regression and correlation analysis from Pearson's technique. Performance of the relative permittivity was evaluated by calculating: (1) standard deviation and (2) root mean square error (RMSE). Where RMSE was determined using

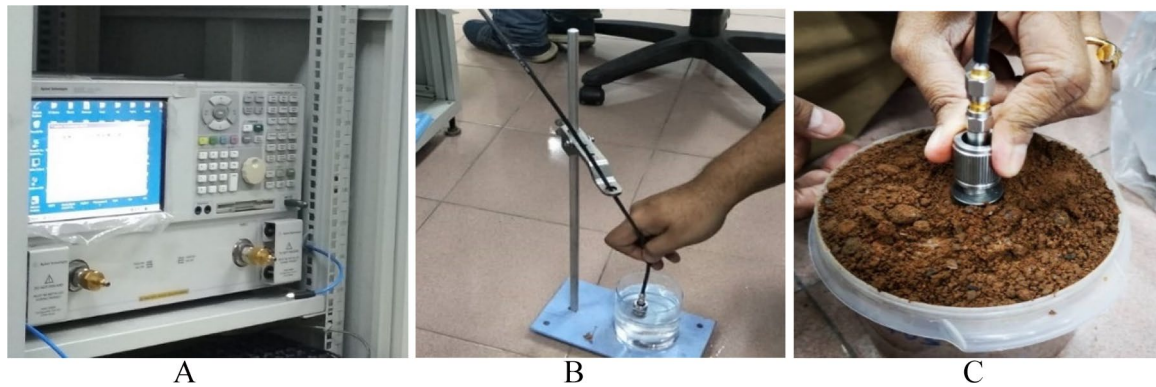


Figure 3. VNA measurement: (A) Automated Vector Analyser, (B) liquid (plain water) reference calibration kit, and (C) measurement of relative permittivity on Terap Red soil sample. VNA indicates automated vector analyser.

$$RMSE = \sqrt{\sum_{i=1}^N (\epsilon_{VNA} - \epsilon_{MEASURED})^2} \quad (4)$$

where N is the number of samples, $\epsilon_{MEASURED}$ is the relative permittivity obtained from GPR measurement, and ϵ_{VNA} is the relative permittivity obtained from the VNA measurement.

Verification of soil relative permittivity by independent GPR

The Terap Red soil was influenced by diesel contamination. In an attempt to obtain effective outcomes for the soil, the relative permittivity of the moisture in the Terap Red soil was evaluated using a permittivity analysis probe which involved an Agilent Technologies Automated Vector Analyser E8562B (VNA). A series of calibrated test automated inversion software which converted the signal was measured into a complex spectrum in a laboratory at Advance Communication Centre (ACE), Pengkalan Jaya Kangar, UNIMAP. This technique was used to measure the actual relative permittivity of subsurface soil as a reference to the independent relative permittivity of the GPR. It could be regarded that the VNA measurements provided the 'true' permittivity values for the assessment of the GPR data.²⁷ Several published studies have proven the superior use of VNA to validate the relative permittivity from the independent GPR. The same case went for Pellinen et al²⁸ study, which performed a comparison of relative permittivity between VNA and GPR measurements on an asphalt pavement specimen, as calibrated with the relative permittivity value from GPR. Meanwhile, a study by Mishra et al²⁹ focused on the calibration of the calculated permittivity behaviour of kaolin suspensions in the tap and deionised water, which was based on the equation of Complex Refractive Index Model (CRIM) through VNA. Prior to the permittivity measurement cell with soil samples, multiline TRL (Thru, Reflect, Line) calibration procedure was implemented to VNA measurement port to minimise any systematic errors. The calibrations consisted of traditional Short-Open-Match reference calibration kit, which was connected between the antenna feed point and

the cable, as shown in Figure 3B. As for the referenced liquid used in the calibration standard, it should be a liquid with 'known' permittivity, such as plain water ($\epsilon = 81$).

Result and Discussion

Interpretation of GPR image

B-scan radar facies by the 800 MHz GPR were collected immediately with the overlapping orthogonal grid prior to and after injection of all diesel amount. The velocity propagation of processed data was calibrated from the hyperbola generated by the inclusion of a PVC with 0.5 m depth, specifically $v = 0.0639$ m/s. Figure 4A presents the results of a processed GPR reflection profile which were collected along Line x2. This coincided with a segment of the moisture test profile. The x2 profile briefly represented the centre line of the gridline area, which was perpendicular with the embedded pipeline location. At this point, the actual mid-location was found, where 10 mm of the hole was pre-drilled under the leaking diesel fuel, leading to the pathway for diesel migration. As the migration of diesel took place through the soil column, the GPR reflection profile changed remarkably, proving the diesel dispersion, which occurred between 5 minutes of experiment time. This event is supported by Mansi et al¹² and Srigutomo and Augustine,¹⁶ as it's driven by the diversity of volumetric moisture content of the soil, the bulk density and the specific density of the solid soil particles. However, the field experiment by Klazinga et al³⁰ was showed no significant amplitude response for sand contaminated by methane release due to lack of relative permittivity contrast from less gas saturation in sand from early leakage detection.

Along with the GPR reflection of x2 profile obtained after 3 hours of measurement as shown in Figure 4B, three difference reflection patterns were displayed. As PVC pipe was injected through the soil column, the first type of reflection appeared between 0.8 and 1.2 m depth, with 1.8 and 2.3 m horizontal distance. These measurements clearly indicated that diesel dispersion started to stagnate from the diesel-soil plume, with an approximate depth of 0.4 m from the pipeline. The

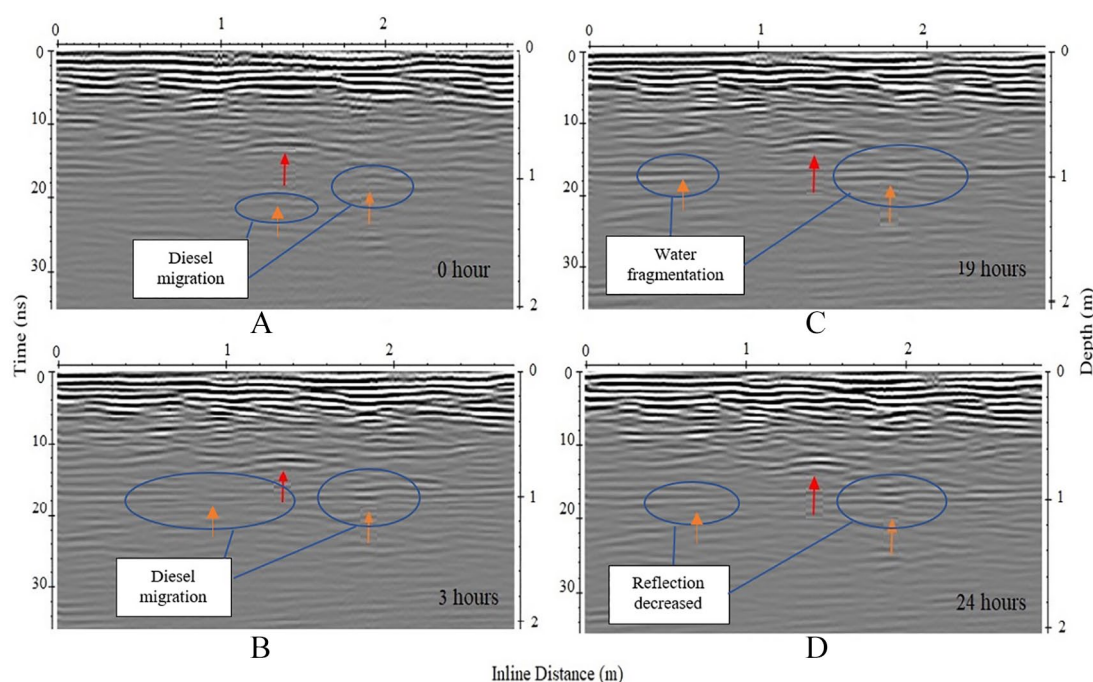


Figure 4. The variation of reflections of the processed GPR data for diesel migration based on temporal difference: (1) red colour arrow representing the pipeline location, and (2) yellow colour arrow representing the diesel migration and (3) blue circle represent GPR reflection which has been influenced by diesel leakage. GPR indicates ground penetrating radar.

second clear indications from the signal reflectivity pattern were the ranges of horizontal distance, which amounted to 1.6 to 1.9 m and 0.7 to 1.0 m depth. Although the third reflection pattern was vertically obtained from 0.8 to 1.6 m range of horizontal distance 0.7 m, while the 0.8 m depth and downwards was obtained during the first hour after diesel injection. Strong reflection zones were currently interpreted as vadose zones, which were distressed by diesel spillage in Terap Red soil, acclimating its moisture content to the surrounding soil. Vlachou et al.³¹ report similar result when observing the resistivity of paraffin oil, whereby distinct regions lag was contributed by a phase of constant initial oil fraction. Contrary occurred in the study of crude oil in underneath thin sea ice by Firoozy et al.,¹⁷ GPR was imaging that the oil eventually migrated upwards towards the sea ice surface. However, there was a weak reflection between the depths of 0.7 to 0.8 m in the first reflection, which was a slight reduction of the signal's effects. Furthermore, weak reflection was indicated from the depth range from 0.8 to 1.0 m in the next column radar facies, which was confirmed by a stronger signal reduction compared to average and interpreted as a more compacted layer. Srigutomo and Agustine¹⁶ also clarified that the weak amplitude signal as result from the existence of LNAPL in the vadose zone above the water table and dominated mixture of oil and water in a silty or clayey environment.

However, significant changes were observed in the weaknesses of reflection after a few hours of observation, and these were indicated from the hyperbola, which was nearly formed through the significant reflections. Figure 4C represents all series of reflection variation patterns, which were slightly

obscured after 19 hours of observation. It could be seen that diesel replaced water pores in a lateral migration with a non-uniform pattern. Furthermore, the non-uniform proliferation of hydrocarbon was illustrated by Mansi et al.,¹² Bano et al.¹⁹ and Abbas et al.,³² which was followed by the production of a new hyperbolic reflection pattern in the hour 19 at a horizontal length between 0.6 and 1.9 m and an approximate depth of 1.0 m. An increasing pattern could be seen with the increase in the wide area, followed by an increase in the range of reflection pattern after 19 hours of diesel migration leakage. A similar result was reported by Klazinga et al.³⁰ and Abbas et al.³² in the monitoring of benzene and methane in a sandy aquifer, after a long period of surveillance, permittivity contrast was formed within the saturated zone resulting in a strong reflection in the GPR profile. To explain the reflection polarity change, it was hypothesised that the fragmentation of water and air regime from soil pores led to enhanced surface runoff and reduced soil moisture. This phenomenon occurred through the replacement of the diesel as soil coating and the remaining water in the outer layer of the diesel fuel as well as pore space. Besides, the deposition of a water-diesel mixture from diesel condensation in humid air at low temperatures at night was another related factor. Compared to Bano et al.,¹⁹ a clear GPR reflection was observed after a duration of diesel contamination in sandy soil due to different soil temperature and sand porosity compared to Terap Red soil, which contributed to significant variations in soil permeability.

Diesel contamination led to a significant increase in the hydrophobicity of the soil as it lost its ability to absorb and retain water on the soil surface, resulting in the decrease in the

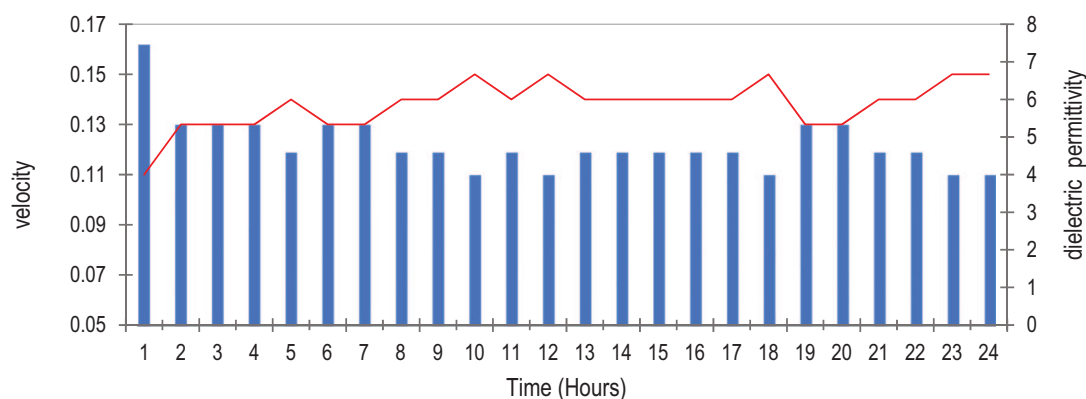


Figure 5. The potential of velocity performance with changes in relative permittivity from GPR data reflection: (1) Red Line representing the velocity alteration and (2) column bar representing the changes in relative permittivity. GPR indicates ground penetrating radar.

GPR reflection amplitude as presented in Figure 4D. As the LNAPLs, diesel is diffused into the saturated zone by increase soil water repellence, flows through the vadose zone until it is trapped within the water table and impermeable layer that associated buoyancy forces arising.^{10,33,34} Meanwhile, the strong amplitude of the waveform on GPR reflection in this zone resulted in the reduction of the electrical conductivity of the soil. It was found that the flow of saturated and dissolved water took place in the stratigraphic of Terap Red soil in slow horizontal motion, with a plumb placed at the centre of gravity. Overall, the majority changes of the reflectivity of GPR radar facies occurred between 20 and 30 ns, which corresponded to a zone consisted of variably connected stratigraphic. Based on this core log, this stratigraphic zone improvised the gain strength of amplitude GPR waveform, which depended on the variation of relative permittivity value.

This region corresponded to the zones of variation of the electrical conductivity and self-control of the shadow zone (low loss-amplitude). These zones could be designated as a region of uniform soil structures, such as Terap Red soil. Another example was humidity, which led to a decrease or absence of permittivity contrast. Therefore, the signal attenuation of GPR reflection was possibly due to the soil-enhanced electrical conductivity, as a result of the degradation processes from diesel migration in soil. Soil contamination led to the local increase in conductivity due to both increasing water content from soil water repellency and evaporation from vaporisation.^{12,35} It was indicated that signal attenuation from electrical conductivity enhancement could cause limited depth penetration of GPR waves. Moreover, GPR signal attenuation related to electrically conductive materials was the primary challenge to overcome.³⁶ However, LNAPLs and DNAPLs compounds presented significantly low electrical conductivity.³⁷ With that being said, GPR was convenient for resistive environments.

It was found that another GPR reflection pattern emerged as a strong straight reflection in the left side, which could be vertically seen in the first 0.40 m along with the profile from the starting point of radarfacies, which horizontally extended until 0.3 m. The identical element took place on the right side

of the x2 profile. This measurement was believed to represent the presence of a concrete wall surface at the survey site. Therefore, it would not be a part of the quantitative interpretation and considered as external interference.

The influence of diesel contamination on EM velocity and soil relative permittivity

According to the estimated radar velocity (0.11 m/ns), there was 5.3 relative permittivity of the clean Terap Red soil body in the survey area. However, there was a constant increase in the Terap Red soil covered by the soil contaminated by the diesel through water replacement. Therefore, polarity contamination propagated consistently with geological observations. This was due to the increase in the radar velocity at the interface between Terap Red soil and diesel (0.13 m/ns with 5.3 relative permittivity). Figure 5 represents the ability of the velocity performance, including the changes in the relative permittivity, which were influenced by the air and pore water replacement in the contaminated zone by diesel as the elements of LNAPL. Diesel fuel with a mass density of 0.830 to 0.836 g cm⁻³ and viscosity at 3.45×10^{-3} Pa s as well as convey relative permittivity value of 2.7 while relative permittivity of water was 80 with mass density of water was 1 g cm⁻³ with dynamic viscosity of water is 8.90×10^{-4} Pa s.^{10,12,33,38} The high velocities estimated near the scattered diesel in sandbox experiment were highlighted by Bano et al.¹⁹ This explained at least partial pore water replacement by the diesel in lateral flow.

Progress was also observed in the amplitude reflection in GPR radarfacies along with the increase in the relative continuation of velocity at 0.15 m/ns from hour 10 onwards. Hewelke et al³³ also mentioned diesel-contaminated soil plume was formed from the hydrophobic nature of hydrocarbons which motivated fractions of soil water holding capacity and water-filled pore space. This incident has contributed to contrast relative permittivity between Terap Red soil layer and the water saturated layer that effected to GPR reflectivity. However, this velocity attenuation was expected due to the increased conductivity and relative permittivity in Terap Red soil, which

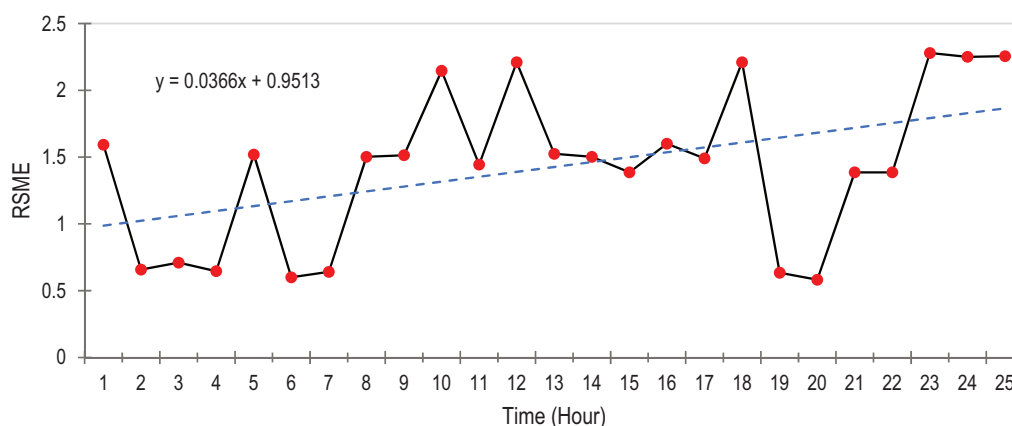


Figure 6. The RMSE of velocity calculated for the differences between the data regarding temporal GPR reflections in diesel-contaminated Terap Red soil. GPR indicates ground penetrating radar. RMSE indicates root mean square error.

was caused by the evaporation of diesel contaminant. This phenomenon was due to the decrease of soil water repellency from degradation processed from soil contamination by LNAPL's which increases total carbon content in soil.^{12,16,33-35} Besides, it migrated vertically into the soil layers. In fact, diesel fuel is recognised to enhance soil hydrophobicity which either fuses into the subsoil (absorption), flows through the subsoil in liquid form, or disappears through leaching (filtration).³⁴

Therefore, the value of relative permittivity decreased over time based on the gradual flow of water, leading to an increase in the velocity and GPR reflection. As presented in Figure 6, the root mean squared errors (RMSEs) of the predicted values of the velocity, which was in relation to the measured value, amounted from 0.001 to 0.05. As shown in a previous study by Yochim et al.,³⁹ the relative permittivity of material influenced the velocity of EM waves and GPR reflection. The size and interaction between the element and the surrounding environment were the influencing factors of the competence of material properties to change the signal of the EM wave, as seen in Figure 6:

The association between soil water content (θ_w) and soil relative permittivity in contaminated soil

The raw soil relative permittivity value was analysed for 24 hours during the soil moisture probes test. In this test, the θ_w was monitored between Terap Red clean soil and diesel-contaminated soil (refer to Figure 7). A positive agreement was observed between the GPR-derived relative permittivity and RSME 0.798, with a measurement of θ_w . The analysis of the correlation coefficient found a remarkable relation ($R=0.813$; $P < .01$) between relative permittivity and the θ_w measured in the Terap Red soil which was contaminated by diesel. A positive correlation was also indicated from the results, suggesting that this GPR measurement was possibly sensitive to different moistures or physical characteristics of the evolving free-phase diesel plume.

Based on a linear regression of the data from the 1.5 m cores through the 24-hour measurement, a strong relationship was

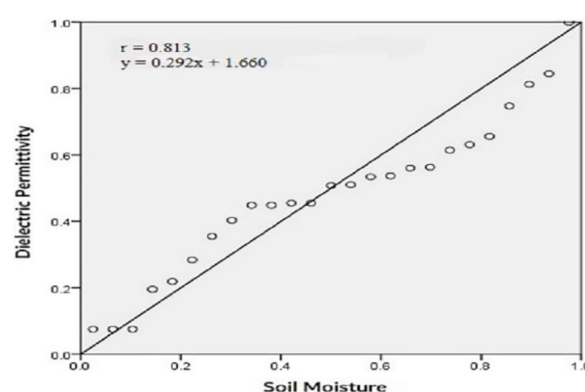


Figure 7. The relationship and correlation between relative permittivity calculated by the GPR data and soil moisture content. GPR indicates ground penetrating radar.

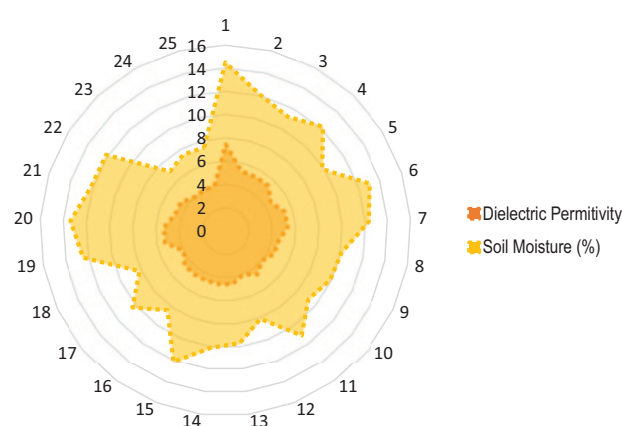


Figure 8. The schematic presentation of the effects of soil moisture on the identification of permittivity constant.

seen between relative permittivity and θ_w : $y=0.292x + 1.660$. As a result of the diesel evaporation interaction particle for EM wave, the interaction of diesel scattered in soil and θ_w . Subsequently, it led to the formation of permittivity-moisture formation network (as shown in Figure 8).

Furthermore, strong regression and schematic presentation show that the increase of soil relative permittivity

with increasing shows the soil relative permittivity is highly dependent on water content. Furthermore, there was a strong relationship between soil relative permittivity and θ_w , as indicated by Topp,³ Roth et al,⁴⁰ Wilczek et al⁴¹ and Rehman and Abouelnaga.⁴² On the other hand, a reflection of amplitude GPR signal from θ_w saturation could be used as an indicator of the diesel which scattered in Terap Red soil which indicated to attenuation of GPR signal amplitudes respective from increased soil electrical conductivity. Furthermore, during diesel contamination, a 'coating' form was produced over soil and covered by water layer. This was followed by the appearance of 'vapour' and 'evaporation', which led to the different relative permittivity of soil. Therefore, the EM wave could be used to obtain contamination, as highlighted by Bano et al¹⁹ and Bradford et al,⁴³ as well as increasing of bulk conductivity over time due to hydrocarbon degradation processes.⁴⁴

It was proven from the clean and contaminated measurements of GPR, that variations of reduction GPR signal amplitudes were affected by migration and chemical reaction of diesel in subsurface. This signal was governed by site-specific nature, including the subsurface material and the interaction between liquid (eg, water and diesel), soil, and antenna system of GPR. To reinforce this argument, the minimum presence of θ_w (7%) in lost factor was influenced by the diesel, which was associated with the calculated soil relative permittivity value of 4. Meanwhile, for the maximum percentage of θ_w 's presence (14.5%), the soil permittivity value amounted to 7.438 (refer to Table 2).

This finding was supported by Abbas et al³² and Cassidy⁴⁵ and in the evaluation of LNAPLs from kerosene, petrol oil and benzene using GPR signal attenuation from hydrocarbon evaporation process that contributed to the variation of relative permittivity. However, Shao et al¹³ were argued in studied on coarse quartz sands (porosity: 46.44%), that time travel of GPR reflected wave was increased due with decrease in the water

level due to water evaporation which leads to relative permittivity decreased. In addition, this study solely focused on the mapping of relative permittivity with little emphasis on the hydrological aspect of diesel reaction in soil.

Therefore, Table 3 and Figure 9 displayed the average relative comparison of the calculated soil relative permittivity by

Table 2. The descriptive statistics of the relative permittivity based on soil moisture test for the processed GPR data.

DESCRIPTIVE STATISTIC	RELATIVE PERMITTIVITY	SOIL MOISTURE
Range	3.438	7.5
Minimum	4	7
Maximum	7.438	14.50
Mean	4.769	10.636
Standard deviation	0.741	2.061
Variance	0.549	4.247

Abbreviation: GPR, ground penetrating radar.

Table 3. The accuracy of average relative permittivity at several depths in the Terap Red soil after fuel injection in comparison to the velocities of GPR waves and VNA.

ACCURACY OF RELATIVE PERMITTIVITY	ACCURACY	
	DIFFERENCE (%)	RMSE
Top core	7.69	0.4
Medium core	4.65	0.2
Bottom core	5.95	0.44

Abbreviation: GPR, ground penetrating radar; RMSE indicates root mean square error; VNA indicates automated vector analyser.

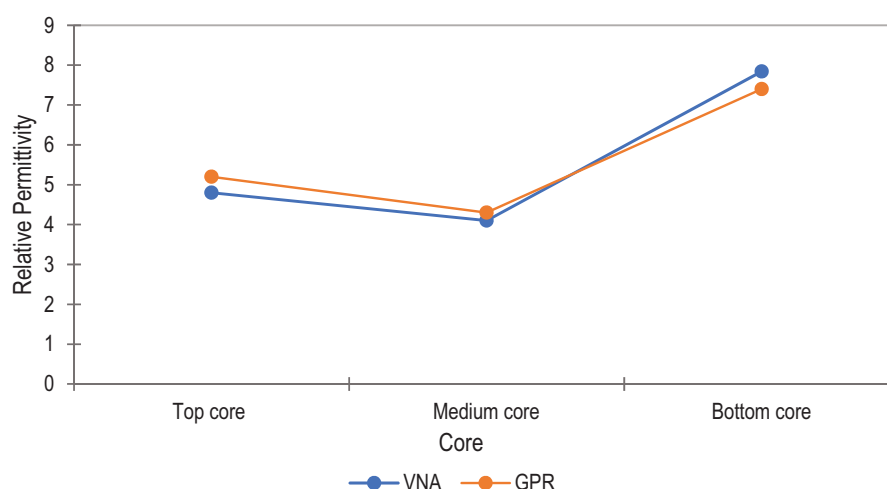


Figure 9. The comparison of average relative permittivity through the estimation of GPR wave and the actual VNA measurement in the Terap Red soil at several depths after fuel injection. GPR indicates ground penetrating radar; VNA indicates automated vector analyser.

processed GPR signal with the calibrated VNA measurement, with a slight difference by 4% to 7% with a total difference of RMSE value amounting to 0.4. It was also shown from the result by VNA that the θ_w affected the formation of soil relative permittivity value. This finding supported the argument presented in Piuze et al⁴⁶ theoretical value that the relative permittivity, which was obtained by GPR, was dependent on θ_w .

Conclusion

This experiment confirms that GPR can be used as a diesel biodegradation monitoring tool for Terap Red soil even in high conductivity environments, despite the amplitude was weakened. Diesel dispersion in Terap Red soil was successful contributed to the GPR reflective response within a short time from diesel leakage compared with the result of sandy or gravel (large porosity) in accordance on literature. Increase in soil water repellency from diesel degradation process which motivated water-filled pore space has contributed to contrast relative permittivity in Terap Red soil that effected strong GPR reflection.

Soil hydrophobicity in Terap Red soil was persuaded to variation of volumetric water content and indirectly influenced to alteration of relative permittivity which has seen by strong relationship in Pearson's statistical analysis. Degradation processed and evaporation from diesel in Terap Red soil was subsidised the conductivity increment and lead to attenuation of GPR amplitude. This locality was also driven to decrease relative permittivity value in the saturated zone. Accuracy of estimated relative permittivity from GPR measurement was proven very precise from actual value from calibrated VNA measurement.

For gain further understanding of the effects of the variable θ_w in a sample of Terap Red soil on EM wave velocity, further research on the empirical model should be done. Potential research apart from investigation for all types of soil contamination, on others application such as subsidence monitoring, sinkhole detection on the carriageway.

Acknowledgements

The authors are grateful to Dr Azremi, the Dean of School of Computer and Communication Engineering, Universiti Malaysia Perlis, for the provision of VNA. The authors would also like to express their gratitude to Universiti Teknologi MARA, Perlis, for the permission given to use the test site in the field and for the funding given by Tabung Amanah Pelajar (TAPA).

Author Contributions

MDG as a research scholar was involved in all stage of research work under supervision OZ and KM. SNAZ was participated in statistical analysis. MNAK working on the calibration experiment. SAA and NFT was contributed to the development of a research proposal. All author substantial contribution to the article and approved the final manuscript.

ORCID iD

Mimi Diana Ghazali  <https://orcid.org/0000-0002-3596-0445>

REFERENCES

- Li Y, Zhou L, Chen J, et al. Dielectric properties of chili powder in the development of radio frequency and microwave pasteurisation. *Int J Food Prop.* 2017;20:3373-3384.
- Awak EA. Determination of soil electrical conductivity using ground penetrating radar (GPR) for precision agriculture. *Int J Sci Eng Res.* 2017;8:1971-1977.
- Topp GC. Electromagnetic determination of soil water content: measurements in coaxial transmission lines. *Water Resour Res.* 1980;16:574-582.
- Brevik EC, Fenton TE, Lazari A. Soil electrical conductivity as a function of soil water content and implications for soil mapping. *Precis Agric.* 2006;7:393-404.
- Karim NIA, Kamaruddin SA, Hasan RC. Modelling of petrophysical relationship of soil water content estimation at peat lands. *Int J Integr Eng.* 2018;10:177-187.
- Sun ZJ, Young GD, McFarlane RA, Chambers BM. The effect of soil electrical conductivity on moisture determination using time-domain reflectometry in sandy soil. *Can J Soil Sci.* 2000;80:13-22.
- Darayan S, Liu C, Shen LC, Shattuck D. Measurement of electrical properties of contaminated soil. *Geophys Prospect.* 2006;46:477-488.
- Ijimdiya TS. Effect of oil contamination on particle size distribution and plasticity characteristics of lateritic soil. In: *Advanced Materials Research.* Vol. 367. Zurich: Trans Tech Publications Ltd; 2012:19-25.
- Naqvi AA, Khari FA, Liadi FA, Raashid MA, Isab AH. Moisture effect in prompt gamma measurements from soil samples. *Appl Radiat Isot.* 2016;115:61-66.
- Bortoni SF, Schlosser RT, Barbosa MC. Numerical modelling of multiphase extraction (MPE) aiming at LNAPL recovery in tropical soils. *Water.* 2019;11:2248.
- Glaser DR, Werkema DD, Versteeg RJ, Henderson RD, Rucker DF. Temporal GPR imaging of an ethanol release within a laboratory-scaled sand tank. *J Appl Geophys.* 2012;86:133-145.
- Mansi AH, Castillo MP, Bernasconi G. Controlled laboratory test for the investigation of LNAPL contamination using a 2.0 GHz ground penetrating radar. *B Geofis Teor Appl.* 2017;58:169-180.
- Shao S, Guo X, Ding H. Temporal Ground Penetrating Radar (GPR) imaging of an oil release within a porous medium: a description of anomalous GPR characteristics during the degradation process and a contaminated area determination method. In: *The International Congress on Environmental Geotechnics.* Singapore: Springer; 2018:850-858.
- Alsharahi G, Driouach A, Faize A. Performance of GPR influenced by electrical conductivity and dielectric constant. *Procedia Technol.* 2016;22:570-575.
- Tillard S, Dubois JC. Analysis of GPR data: wave propagation velocity determination. *J Appl Geophys.* 1995;33:77-91.
- Srigutomo W, Agustine E. Investigation of underground hydrocarbon leakage using ground penetrating radar. *J Phys Conf Ser.* 2016;739:012137.
- Firoozy N, Neusitzer T, Chirkova D, et al. A controlled experiment on oil release beneath thin sea ice and its electromagnetic detection. *IEEE T Geosci Remote.* 2018;56:4406-4419.
- Daniels JJ, Roberts R, Vendl M. Ground penetrating radar for the detection of liquid contaminants. *J Appl Geophys.* 1995;33:195-207.
- Bano M, Loeffler O, Girard JF. Ground penetrating radar imaging and time-domain modelling of the infiltration of diesel fuel in a sandbox experiment. *C R Geosci.* 2009;341:846-858.
- Wu T, Huang R, Chi M, Weng T. A study on electrical and thermal properties of conductive concrete. *Comput Concrete.* 2013;12:337-349.
- United States Department of Agriculture, Natural Resources Conservation Service and Soil Survey Staff. *Soil Taxonomy: A Basic System of Soil Classification for Making and Interpreting Soil Surveys.* 2nd ed. Washington, DC: U.S. Government Printing Office; 1999.
- BS 1377-4:1990. Soils for civil engineering purposes – part 8.
- Salih SA. Applications of Ground Penetrating Radar (GPR) in detection of behaviour of groundwater table near pumping well. *Tikrit J Pure Sci.* 2007;12:192-204.
- Mount GJ, Comas X, Wright WJ, McClellan MD. Delineation of macroporous zones in the unsaturated portion of the Miami Limestone using ground penetrating radar, Miami Dade County, Florida. *J Hydrol.* 2015;527:872-883.
- Dahboosh ASJ. *Investigation of Subsidence Phenomena by GPR Technique and Geotechnical Evaluation in Baghdad City* [PhD thesis]. Baghdad, Iraq: University of Baghdad; 2013.

26. Remke LVD. *Causes of Ground-Penetrating Radar Reflections in Sediment* [PhD thesis]. Amsterdam, The Netherlands: de Vrije Universiteit Amsterdam; 2001.
27. Pellinen T, Eskelinen P, Huuskonen-Snicker E, Hartikainen A. *Assessment of Air Void Content of Asphalt Using Dielectric Constant Measurements by GPR and with VNA*. Helsinki, Finland: Aalto University publication; 2015.
28. Pellinen T, Huuskonen-Snicker E, Eskelinen P, Martinez PO. Representative volume element of asphalt pavement for electromagnetic measurements. *J Traffic Transp Eng (English Edition)*. 2015;2:30-39.
29. Mishra PN, Bore T, Jiang Y, Scheuermann A, Li L. Dielectric spectroscopy measurements on kaolin suspensions for sediment concentration monitoring. *Measurement*. 2018;121:160-169.
30. Klazinga DR, Steelman CM, Endres AL, Parker BL. Geophysical response to simulated methane migration in groundwater based on a controlled injection experiment in a sandy unconfined aquifer. *J Appl Geophys*. 2019;168:59-70.
31. Vlachou MC, Zacharias KA, Kostoglou M, Karapantsios TD. Droplet size distributions derived from evolution of oil fraction during phase separation of oil-in-water emulsions tracked by electrical impedance spectroscopy. *Colloid Surf Physicochem Eng Asp*. 2020;586:124292.
32. Abbas M, Jardani A, Machour N, Dupont JP. Geophysical and geochemical characterisation of a site impacted by hydrocarbon contamination undergoing biodegradation. *Near Surf Geophys*. 2018;16:176-192.
33. Hewelke E, Szatylowicz J, Hewelke P, Gnatowski T, Aghalarov R. The impact of diesel oil pollution on the hydrophobicity and CO₂ efflux of forest soils. *Water Air Soil Poll*. 2018;229:51.
34. McWatters RS, Rowe RK, Wilkins D, et al. Modelling of vapour intrusion into a building impacted by a fuel spill in Antarctica. *J Environ Manag*. 2019;231:467-482.
35. Tomlinson DW, Thornton SF, Thomas AO, Leharne SA, Wealhall GP. *Illustrated Handbook of LNAPL Transport and Fate in the Subsurface*. London, England: Contaminated Land: Applications in Real Environments (CL:AIRE); 2014.
36. Leucci G. Ground penetrating radar: the electromagnetic signal attenuation and maximum penetration depth. *Scholar Res Exchange*. 2008;2008:926091.
37. Chala AT, Matula S, Bátková K, Doležal F. Evaluation of methods for water and non-volatile LNAPL content measurement in porous media. *Soil Water Res*. 2019;14:47-56.
38. Wang P, Hu Z, Zhao Y, Li X. Experimental study of soil compaction effects on GPR signals. *J Appl Geophys*. 2016;126:128-137.
39. Yochim A, Zytner RG, McBean EA, Endres AL. Estimating water content in an active landfill with the aid of GPR. *Waste Manag*. 2013;33:2015-2028.
40. Roth K, Schulm R, Flüßler H, Attinger W. Calibration of time domain reflectometry for water content measurement using a composite dielectric approach. *Water Resour Res*. 1990;26:2267-2273.
41. Wilczek A, Szyplowska A, Lewandowski A, Kafarski M, Szerement J, Skierucha W. Soil salinity characterization based on 0.05–3 GHz dielectric permittivity measurements. Paper presented at: IEEE MTT-S International Microwave Workshop Series on Advanced Materials and Processes for RF and Thz Applications, IMWS-AMP; September 20–22, 2017; Pavia, Italy. New York: IEEE: 1-3.
42. Rehman F, Abouelnaga HSO. Estimation of dielectric permittivity, water content, and porosity for environmental engineering and hydrogeological studies using ground penetrating radar, a short review. *Arab J Geosci*. 2016;9:1-7.
43. Bradford JH, Babcock EL, Marshall HP, Dickins DF. Targeted reflection-waveform inversion of experimental ground-penetrating radar data for quantification of oil spills under sea ice. *Geophysics*. 2016;81:59-70.
44. Kimak C, Ntarlagiannis D, Slater LD, et al. Geophysical monitoring of hydrocarbon biodegradation in highly conductive environments. *J Geophys Res-Bioge*. 2019;124:353-366.
45. Cassidy NJ. Evaluating LNAPL contamination using GPR signal attenuation analysis and dielectric property measurements: practical implications for hydrological studies. *J Contam Hydrol*. 2007;94:49-75.
46. Piuze E, Cannazza G, Cataldo A, et al. A comparative assessment of microwave-based methods for moisture content characterization in stone materials. *Measurement*. 2018;114:493-500.